Influence of Minor Alloying Elements on Selective Oxidation and Reactive Wetting of CMnSi TRIP Steel during Hot Dip Galvanizing

LAWRENCE CHO, MYUNG SOO KIM, YOUNG HA KIM, and BRUNO C. DE COOMAN

The influence of the addition of minor alloying elements on the selective oxidation and the reactive wetting of CMnSi transformation-induced plasticity (TRIP) steels was studied by means of galvanizing simulator tests. Five TRIP steels containing small alloying additions of Cr, Ni, Ti, Cu, and Sn were investigated. After intercritical annealing (IA) at 1093 K (820 °C) in a N_2 + 5 pct H_2 gas atmosphere with a dew point of 213 K (−60 °C), two types of oxides were formed on the strip surface: Mn-rich xMnO·SiO$_2$ ($x > 1.5$) and Si-rich xMnO·SiO$_2$ ($x < 0.3$) oxides. The addition of the minor alloying elements changed the morphology of the Si-rich oxides from a continuous film to discrete islands and this improved the wettability by molten Zn. The improved wetting effect of the minor alloying elements was attributed to an increased area fraction of the surface where the oxides were thinner, enabling a direct unhindered reaction between Fe and the Al in the liquid Zn and the formation of the inhibition layer during the hot dip galvanizing. The addition of a small amount of Sn is shown to significantly decrease the density of Zn-coating defects on CMnSi TRIP steels.

DOI: 10.1007/s11661-014-2394-y

I. INTRODUCTION

THE gas atmosphere in annealing furnaces of continuous hot dip galvanizing (HDG) lines reduces the iron oxides formed during cold rolling to elemental Fe. The alloying elements, Mn, Si, and Al are subject to selective oxidation since they have a high affinity for oxygen. This selective oxidation occurs at the steel surface in the low dew point (DP) annealing furnace gas atmosphere of HDG lines operated in standard conditions. The presence of film-forming surface oxides, in particular amorphous ***a***-xMnO·SiO$_2$ ($x < 0.9$) and ***a***-SiO$_2$ oxides, leads to a deterioration of the wettability of the intercritically annealed strip by the molten Zn and prevents the formation of the $Fe_2Al_{5-x}Zn_x$ inhibition layer at the steel surface.[1–4] This selective oxidation phenomenon occurring at the surface and in the subsurface of most industrial steel grades has been investigated in detail for interstitial-free steel, dual phase steel, and transformation-induced plasticity (TRIP).[5–7]

The four methods which have been proposed to improve the quality of the hot dip Zn coatings are shown in Figure 1. The first method consists of annealing the strip in a high DP atmosphere, which results in internal oxidation rather than external oxidation.[1,2,8] The second method is a two step procedure consisting of an oxidation followed by a reduction.[9–12] In the oxidation stage, the surface is fully oxidized to a Fe-oxide layer. The Mn, Si, and Al, which diffuse to the interface between the ferrite and the Fe-oxide layer, form compound oxides. In the reduction stage, the Fe oxide is fully reduced to a pure Fe layer with embedded selective oxides. The third method involves the deposition of a thin layer of pure Fe, Ni, or Cu prior to the annealing stage in HDG lines.[13–15] The fourth method involves the addition of surface active elements such as Sn and Sb to the steel composition. These elements tend to segregate to grain boundaries and the surface during annealing. When these elements segregated on the surface, they suppress the surface oxidation by occupying the oxygen adsorption surface sites.[16–18]

The fourth method, *i.e.*, the addition of surface active elements, is potentially the easiest to implement industrially, as the other methods involve a modification to the parts of the industrial lines. However, the research on the use of this approach to the galvanizing industry is in the initial stages and the method has not been verified using industrial annealing conditions. Furthermore, the mechanism of the oxidation retardation by addition of these elements has not been fully documented.

In the present paper, the surface oxides formed during the annealing of five TRIP steels containing small additions of Cr, Ni, Ti, Cu, and Sn were therefore analyzed by means of high resolution transmission electron microscopy (TEM) of cross-sectional samples

LAWRENCE CHO, Graduate Student, is with Materials Design Laboratory, Graduate Institute of Ferrous Metallurgy, Pohang University of Science and Technology, Pohang 790-784, South Korea. MYUNG SOO KIM and YOUNG HA KIM, Research Staff Members, are with POSCO Technical Research Laboratories, Gwangyang 545-090, South Korea. BRUNO C. DE COOMAN, Professor, is with Graduate Institute of Ferrous Metallurgy, Pohang University of Science and Technology, and also Director, with Materials Design Laboratory, Pohang University of Science and Technology. Contact e-mail: decooman@postech.ac.kr

Manuscript submitted October 25, 2013.
Article published online June 18, 2014

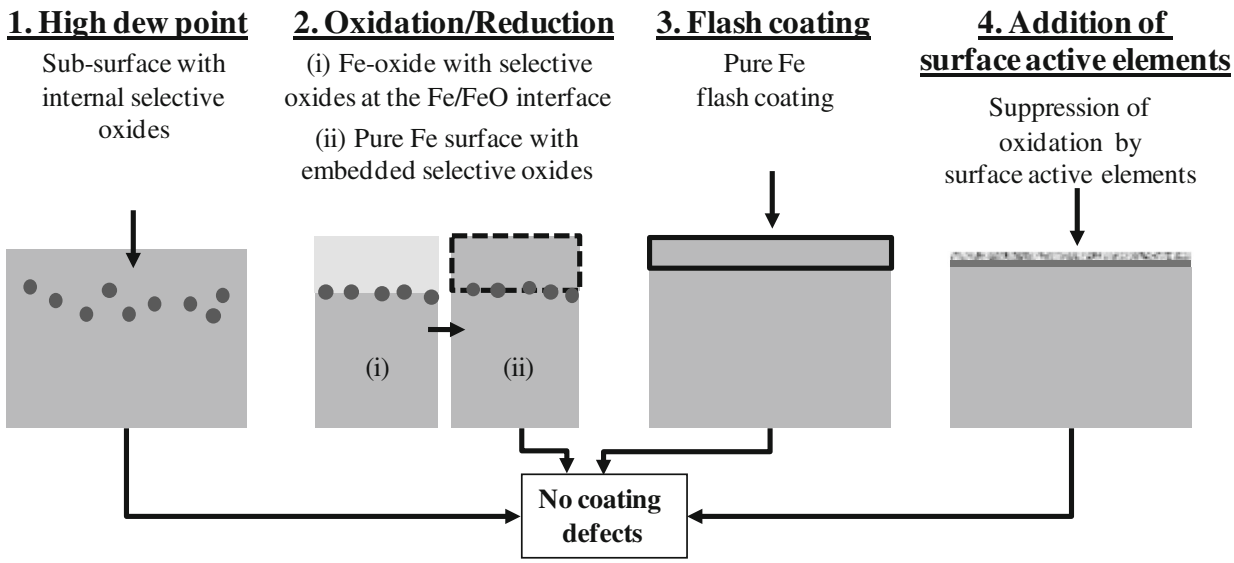

Fig. 1—Schematic of the four methods proposed to prevent formation of Zn-coating defects resulting from presence of surface selective oxides formed during annealing prior to the hot dip galvanizing of AHSS steel.

prepared by the focused ion beam (FIB) technique. The galvanizability and wettability of the intercritically annealed TRIP steels were examined. The effect of each element on the selective oxidation during the annealing and on the reactive wetting during the hot dipping was analyzed.

II. ALLOY DESIGN

Ruck *et al.*[19] studied effects of several tramp elements on the carburization rate of steel. They reported that carburization was much slower for steels alloyed with Sn or Sb and concluded that the efficiency of an element to suppress the surface reaction is associated with its tendency for surface segregation. In order to test if the same mechanism could be applied to the oxidation behavior, some alloying elements were selected as alloying additions, and the degree of surface segregation of these alloying elements was evaluated.

The degree of grain boundary or surface segregation of an element was discussed by Seah.[20] He defined the surface enrichment factor of a solute atom A in a solvent atom B, β_A^S as follows:

$$\beta_A^S = \frac{X_S}{1 - X_S} \cdot \frac{1 - X_B}{X_B}, \qquad [1]$$

where X_S is fractional coverage of the surface of the solute atom A and X_B is bulk mole fraction of the solute atom A. Seah[20] provided the following equation for the calculation of β_A^S:

$$\ln \beta_A^S = \left\{ 24\left(T_B^m - T_A^m\right) + 1.86\Omega + M4.64 \cdot 10^7 a_B (a_A - a_B)^2 \right\} / RT \pm 1.29. \qquad [2]$$

Here, T is the temperature, T_A^m and T_B^m are melting temperatures (T_m) of the pure solids A and B, respectively. Ω is the mixing enthalpy of A and B. a_A and a_B are atomic sizes of A and B. $M = 1$ for $a_A > a_B$ and $M = 0$ for $a_A < a_B$. The main contribution to the driving force for surface segregation in Eq. [2] is the reduction of the surface energy when the matrix surface is covered with a layer of solute A atoms. In Eq. [2], the difference in T_m is used because it is closely related to the surface energy and the values of T_m are accurately known. The second contribution to the driving force for segregation is the atomic size difference; here, the driving force is due to the lowering of the elastic strain energy in the bulk which arises from lattice mismatch. Tsai *et al.*[21] argued that the elastic energy driving force may be appreciably smaller for an undersized solute atom than for an oversized solute atom, even though the absolute difference in atomic volumes of the pure components, are the same. Seah[20] therefore assumed that $M = 0$ when the solute atom size was smaller than the solvent atom, *i.e.*, $a_A < a_B$.

Figure 2 shows a plot for T_m for Fe and segregant elements as a function of their atomic size, calculated by means of the following equation.[22]

$$a = \sqrt[3]{\frac{A}{\rho \cdot N}}. \qquad [3]$$

Here, A is the atomic weight of the element, ρ is the bulk density of the pure material, and N is Avogadro's number. Figure 2 shows that, in an α-Fe matrix, the surface enrichment factors of Bi, Sn, Sb, and S atoms are expected to be high as they have a lower T_m and an atomic size that is larger than Fe. In contrast, the surface enrichment factors for Ni, Cu, Cr, and Ti are predicted to be low as they have similar atomic size to Fe.

The present study focuses on the effect of five elements, Cr, Ni, Ti, Cu, and Sn. Cr and Ni were chosen as the reference solutes. According to Eq. [1], Cr

is expected to have low surface segregation tendency when present as a solute in an Fe matrix because it has a higher T_m than Fe and a similar atomic size. Ni, whose T_m and atomic size are similar to those of Fe, is also expected to have a low surface segregation tendency. Although the atomic size of Ni is slightly smaller than that of Fe, the effect of the elastic energy driving force for the undersized solute atom is negligible, as has been suggested by Tsai *et al.*[21] Ti, has a larger atomic size than Fe, and is expected to have a high surface segregation tendency. Cu has a T_m lower than Fe, and

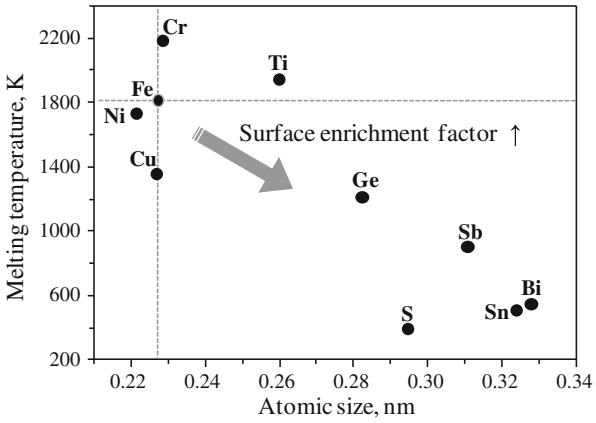

Fig. 2—Melting temperature of selected elements as a function of their atomic sizes.

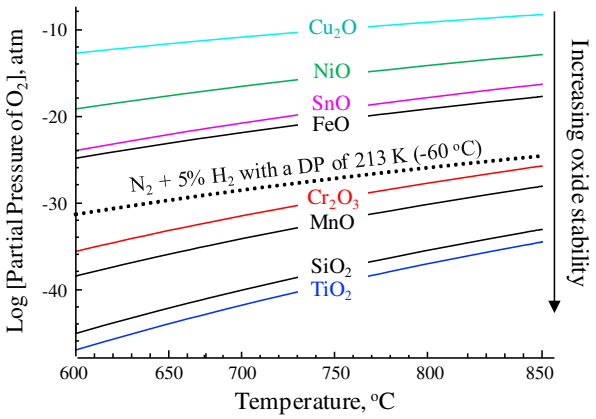

Fig. 3—Temperature dependence of the equilibrium oxygen partial pressure for the binary metal oxides/metal systems.

is also expected to have a strong tendency for surface segregation. Sn has both a low T_m and a larger atomic size. It is expected to be a surface active element with a large surface segregation tendency. Based on Eq. [2], the tendency for the surface segregation can be ordered as follows: Sn > Ti ≈ Cu > Ni ≈ Cr.

If an element has a high affinity to oxygen, selective oxidation of the element can also result in its surface enrichment. If an element forms oxides and is depleted near the surface, this depletion leads to concentration gradient. Consequently, the elements will diffuse to the surface to form oxides. The stability of the oxides for the annealing conditions used for the present study is shown in Figure 3. It shows the temperature dependence of equilibrium oxygen partial pressure for the metal oxides/metal systems. The Gibbs oxide formation energy given by Lee[23] was used for the calculation. For the conditions located below each curve, the oxide is unstable, while, above the curve, the metal is oxidized. The oxygen partial pressure used for the present study is indicated by the dashed line in the diagram. While Ni, Cu, and Sn have a low oxidation tendency, Cr and Ti have a high affinity to oxygen, and they will readily form oxides in the annealing conditions. In certain conditions, Ti may also be present as TiC or TiN, rather than remain in solid solution. Therefore, the additional effects of precipitation and oxidation were also investigated in the present work.

Table I lists the chemical compositions of CMnSi TRIP steels used in the present study. One reference-TRIP steel and five TRIP steels with additions of 0.3 mass pct Cr, 0.3 mass pct Ni, 0.02 mass pct Ti, 0.3 mass pct Cu, and 0.05 mass pctSn were selected. Suzuki *et al.*,[24] who calculated the chemical potential diagram for Fe-Mn-Si-O system, suggested that when the Si/Mn mass pct ratio of the steel composition was higher than 1, the galvanizability was poor due to the formation of SiO_2. Therefore, the reference-TRIP steel, containing 1.6 mass pct Mn and 1.5 mass pct Si, is expected to have poor galvanizability. The C, Mn, and Si contents of the six steels were comparable. The alloying levels of the minor elements were low in order to limit the possibility that the element would form precipitates or affect the mechanical properties. As it has been reported that Cr affects the bainitic transformation, the Cr content was limited to 0.3 mass pct.[25] Cu and Ni added in excess of 0.5 mass pct alter the microstructure and the mechanical properties of the continuous-annealed steel.[25] The Cu and Ni content were therefore limited to 0.3 mass pct. The Ti content

Table I. Chemical Compositions of the Reference-TRIP Steel and the 0.3 pctCr-Added, 0.3 pctNi-Added, 0.02 pctTi-Added, 0.3 pctCu-Added, and 0.05 pctSn-Added TRIP Steels

Alloy Name	C	Mn	Si	Cr	Ni	Ti	Cu	Sn
Reference-TRIP	0.1	1.6	1.5					
0.3 pctCr-added	0.1	1.6	1.5	0.3				
0.3 pctNi-added	0.1	1.6	1.5		0.3			
0.02 pctTi-added	0.1	1.6	1.5			0.02		
0.3 pctCu-added	0.1	1.6	1.5				0.3	
0.05 pctSn-added	0.1	1.6	1.5					0.05

was limited to 0.1 mass pct in order to avoid a significant reduction in formability.[26] A low content of Sn, 0.05 mass pct, was chosen because Sn is known to cause hot shortness, a lack of ductility due to the presence of a molten phase at grain boundaries.[27]

III. EXPERIMENTAL

Industrially cold-rolled full-hard reference-TRIP steel and 0.3 pctCr-added, 0.3 pct Ni-added, 0.02 pctTi-added, 0.3 pctCu-added, and 0.05 pctSn-added TRIP steels were used for the present work. The dimensions of the sheet panels used for the annealing and the Zn hot dipping experiments were 220 mm in length, 120 mm in width, and 1.0 mm in thickness. The samples were intercritically annealed in an IWATANI SURTEC HDG simulator manufactured by IWATANI Inc. This HDG simulator consists of a main unit, a gas mixing station, a hybrid humidification system, and a control system. The infra-red furnace in the main unit was used for the continuous intercritical annealing (IA) simulation. The process gasses, N_2, H_2, and He, were mixed in the gas mixing station and the gas mixture was humidified in the hybrid humidification system. The control system allowed for the precise control of the composition of the gas atmosphere.

The continuous annealing simulation was carried out at an IA temperature of 1093 K (820 °C) in a N_2 + 5pctH_2 gas atmosphere with a DP of 213 K (−60 °C). Huin *et al.*[28] provided a formulae to calculate the oxygen partial pressure (P_{O_2}) of a gas atmosphere containing water vapor. The P_{O_2} at the IA temperature in this atmosphere was calculated to be 5.16×10^{-26} atm. Prior to the continuous annealing simulation, small coupons of 15×15 mm^2 taken from larger panel samples were mirror-polished with a 1 μm diamond suspension in order to allow for cross-sectional TEM observations which are not influenced by the sheet surface roughness.

Figure 4 shows the thermal cycle for the experiments. The annealing consisted of heating at a heating rate of +3 K/s to the IA temperature of 1093 K (820 °C). The panels were held at the IA temperature for 47 seconds, slow cooled with a cooling rate of −3 K/s to 943 K (670 °C), rapidly cooled using a cooling rate of −17.6 K/s to the isothermal bainitic transformation (IBT) temperature of 673 K (400 °C), and held at the IBT temperature for 120 seconds prior to a final rapid cooling to room temperature with N_2 gas with a cooling rate of −20 to −30 K/s.

The morphology of the surface oxides formed during the continuous annealing was investigated by scanning electron microscopy (SEM) and TEM. The surface of the annealed sample was analyzed in a ZEISS ULTRA-55 field emission (FE) SEM operated with an accelerating voltage of 10 keV. The cross-sectional TEM samples were prepared by the FIB technique in a FEI Quanta 3D FEG. The TEM samples were analyzed in a JEOL JEM-2100F FE-TEM operated at 200 keV. The oxide composition was determined by means of energy dispersive spectroscopy (EDS) using a 10 nm diameter

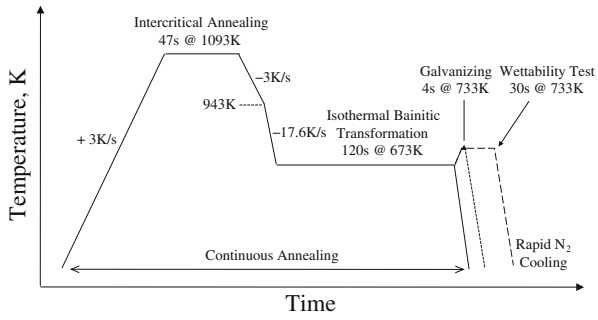

Fig. 4—Schematic of the continuous annealing cycle.

electron beam. Ten measurements taken in the oxide layer were averaged to determine the mean composition of the oxides.

Depth profiles of the chemical composition of the surface of the annealed samples were obtained with a LECO GDS-850A glow discharge optical emission spectrometer (GDOES). The GDOES analysis was done using a voltage of 700 V, a constant current of 20 mA, and an Ar pressure in the range of 9 to 13 hPa. The analyzed area was approximately 4 mm in diameter. A CAMECA IMS6F was used for the secondary ion mass spectroscopy (SIMS) analysis using an 8 keV O_2^+ source. The analyzed area was approximately 60 μm in diameter.

Two sets of experiments were carried out to investigate the galvanizability of the intercritically annealed steels: (i) galvanizing simulation carried out in an IWATANI SURTEC HDG simulator and (ii) wetting force measurement, carried out in a RHESCA force balance simulator. The thermal cycle for both experiments was based on the same heating cycle as the one used for the continuous annealing simulation (Figure 2) prior to a hot dipping in the liquid Zn bath. The Zn bath temperature was 733 K (460 °C) and the total Al content of the liquid Zn was 0.22 mass pct. Prior to the galvanizing simulation, the sheets were degreased with kerosene, ultrasonically cleaned in ethanol and acetone to remove lubricant residues and iron fines. After the continuous annealing simulation, the samples were dipped in the liquid Zn bath for 4 seconds and rapidly cooled to room temperature with N_2 gas. The dipping direction of the samples was perpendicular to the rolling direction.

Prior to the wetting force measurement, small coupons of 20×50 mm^2 were taken from larger panel samples. Both sides of the samples surface were mirror-polished with a 1 μm diamond suspension in order to eliminate the roughness effects during the experiment. After the continuous annealing simulation, the wetting force was measured while the samples were dipped in the liquid Zn bath for 30 seconds.

The normalized wetting force was computed by means of the following equation[29]:

$$\gamma_{LV} \cos\theta = \frac{F_{measured} - m \cdot g + V_{displaced} \cdot \rho_{bath} \cdot g}{P}. \quad [4]$$

Here, $\gamma_{LV}\cos\theta$ is the wetting force normalized by the sample cross section perimeter P, $V_{displaced}$ is the liquid Zn volume displaced by the sample, ρ_{bath} is the Zn bath density, γ_{LV} is the surface tension of the Zn bath, and θ is the contact angle.

IV. RESULTS

A. *Morphology and Chemical Composition of the Surface Oxides*

Figure 5 shows GDOES elemental depth profiles for the surface and the subsurface of the six TRIP steels after IA in a N_2 + 5 pct H_2 gas atmosphere with a DP of 213 K (−60 °C). The Mn and Si concentration profiles were similar in all cases. The formation of Si oxides occurred over a smaller thickness range than the formation of Mn oxides. The maximum enrichment of Si was found at a depth of approximately 5 nm, while that of Mn was in the depth range of 10 to 15 nm. The oxidation depth was around 30 nm in both cases. The GDOES data clearly show the formation of a segregation layer of the minor alloying elements near the surface. There was a slight segregation of Cr on the surface of the intercritically annealed 0.3 pctCr-added TRIP steel (Figure 5(b)). But, Cr was mostly enriched beneath the xMnO·SiO$_2$ surface oxide layer. Ni

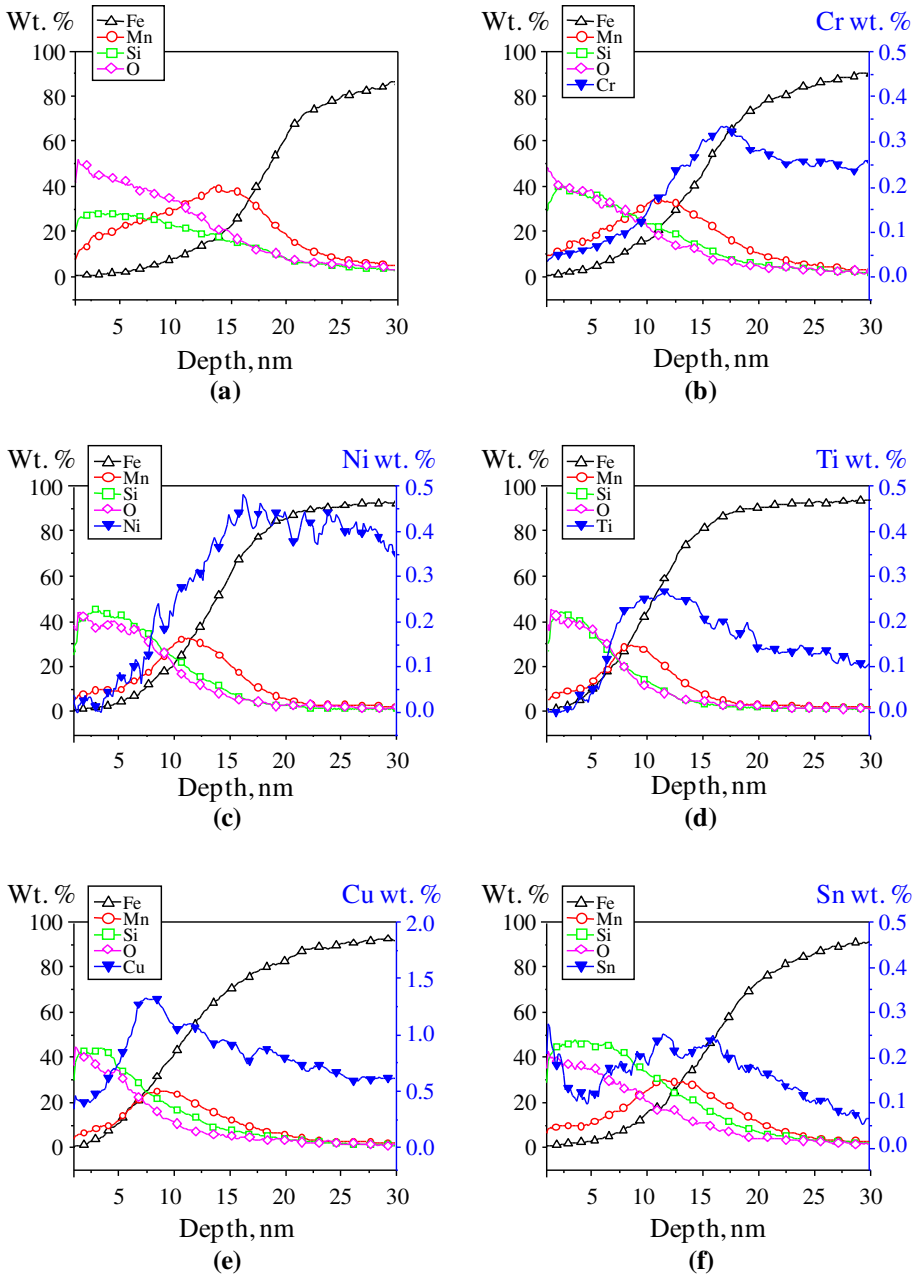

Fig. 5—GDOES depth profiles for Fe, Mn, Si, O, Cr, Ni, Ti, Cu, and Sn on the surface of (*a*) the reference-TRIP steel and (*b*) the 0.3 pctCr-added, (*c*) 0.3 pct Ni-added, (*d*) 0.02 pctTi-added, (*e*) 0.3 pctCu-added, and (*f*) 0.05 pctSn-added TRIP steels.

remained in solid solution. A very low Ni surface enrichment was observed in the case of the intercritically annealed 0.3 pctNi-added TRIP steel (Figure 5(c)). Ti was mainly present as precipitate, TiC or TiN. Some of the solute Ti segregated to the surface of the intercritically annealed 0.02 pctTi-added TRIP steel (Figure 5(d)). Ti is known to form the very stable TiO_2 oxide. The surface enrichment was therefore very likely due to TiO_2 formation. Cu was significantly enriched at the surface of the intercritically annealed 0.3 pctCu-added TRIP steel (Figure 5(e)). The depth where the enrichment of Cu reached a maximum was intermediate between the depth of maximum enrichment for Si and Mn. This indicates that a large degree of surface segregation for Cu. Although the Sn alloying addition was small, the surface segregation of Sn was exceptionally large. The enrichment of Sn was mostly observed on the surface oxides (Figure 5(f)). This observation indicates that Sn segregation occurred before the selective oxidation of Mn and Si started.

Figure 6 shows xMnO·SiO_2 oxides formed on the surface of the TRIP steels during IA in a N_2 + 5 pct H_2 gas atmosphere. The morphology of the oxides was significantly influenced by addition of minor alloying

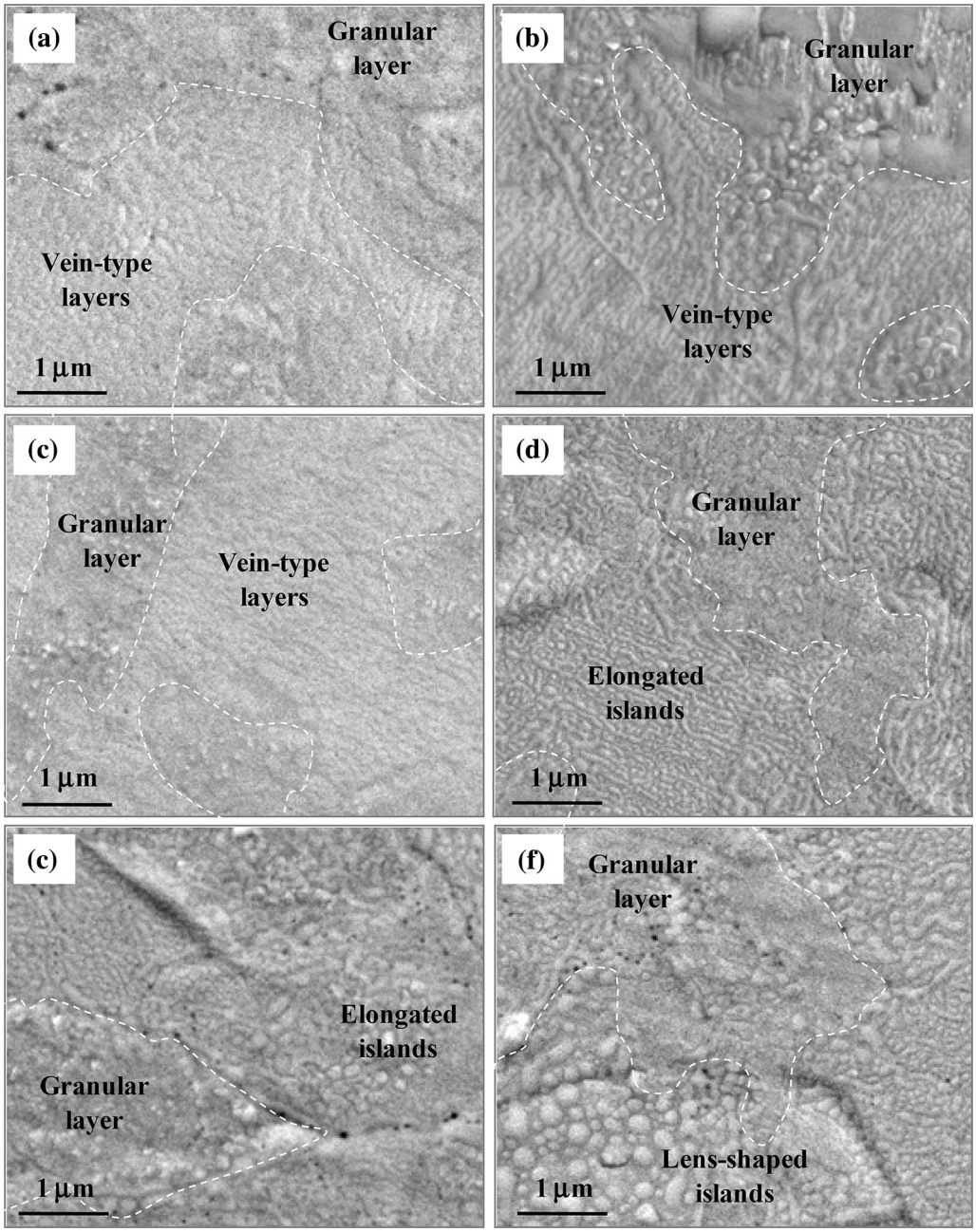

Fig. 6—SEM micrographs of the xMnO·SiO_2 oxides formed on the surface during intercritical annealing of the six CMnSi TRIP steels: (*a*) reference-TRIP, (*b*) 0.3 pctCr-added, (*c*) 0.3 pctNi-added, (*d*) 0.02 pctTi-added, (*e*) 0.3 pctCu-added, and (*f*) 0.05 pctSn-added TRIP steels.

elements. In general, the morphology of the oxide layers changed from continuous layers on the reference-TRIP steel to a discrete island morphology on the alloyed TRIP steels. Continuous oxide layers with a characteristic vein-like morphology were formed on the surface of the reference-TRIP steel and the 0.3 pctCr-added TRIP steel (Figures 6(a) and (b)).The oxide layers appeared to form networks. Two types of the oxide layers were formed at the surface of the 0.3 pctNi-added TRIP steel (Figure 6(c)). One was a granular oxide layer. The other had a vein-type morphology. The thickness of the vein-type oxide layer was thinner than on the reference-TRIP steel and the 0.3 pctCr-added TRIP steel. Elongated oxide islands were formed at the surface of the 0.02 pctTi-added TRIP steel and the 0.3 pctCu-added TRIP steel (Figures 6(d) and (e)). The addition of Sn dramatically changed the morphology of the oxides, which were lens-shaped, with a radius in the range from 50 to 200 nm (Figure 6(f)).

Figure 7 shows a schematic for the three types of oxide morphologies formed on the surface of the TRIP steels during IA. Vein-type oxide layers and granular oxide layers were formed on the reference-TRIP steel, the 0.3 pctCr-added TRIP steel and the 0.3 pctNi-added TRIP steel (Figure 7(a)). Elongated oxide islands and granular oxide layers were formed on the 0.02 pctTi-added TRIP steel and the 0.3 pctCu-added TRIP steel (Figure 7(b)). Lens-shaped oxide islands and granular oxide layers were formed on the 0.05 pctSn-added TRIP steel (Figure 7(c)).

TEM was used to investigate the morphology of the xMnO·SiO$_2$ oxides at high resolution. Figure 8 shows cross-sectional TEM micrographs of the oxides formed at the surface of the reference-TRIP steel. Note that Pt and Au layers were deposited prior to the FIB sample preparation to protect the surface. In the TEM micrographs the thicker upper layer and the thinner lower layer with a dark contrast are Pt and Au coatings, respectively. The Ti K_α peak in the EDS spectra is from the Ti TEM sample grid. The surface oxide layer was continuous. Two types of the surface oxides were formed: Si-rich xMnO·SiO$_2$ (x = 0.18) and Mn-rich xMnO·SiO$_2$ (x = 1.75) oxides. The observation that two types of oxides formed separately during IA of the reference-TRIP steel is consistent with the results of an earlier study.[3] The Si-rich oxide layers and the Mn-rich oxide layers correspond to the vein-type oxide layer and the granular oxide layer, respectively, observed in SEM (Figure 6(a)).

Figure 9 shows cross-sectional TEM micrographs of the oxides formed on the surface of the 0.3 pctNi-added TRIP steel during IA. In some areas, the oxide layer was very thin compared to that of the reference-TRIP steel (Figure 9(b)). The average Mn/Si atomic ratio, x, of the oxide layer was 1.75. However, it was not reliable as the count level of the EDS result was too small and the standard deviation was too high (Figure 9(d)). In other parts, thicker oxide layers were formed (Figure 9(c)). These layers were Mn-rich xMnO·SiO$_2$ (x = 1.55) oxides (Figure 9(e)). The thin and thick oxide layers correspond to the vein-type oxide layer and the granular oxide layers, respectively.

Figure 10 shows cross-sectional TEM micrographs of the oxides formed on the surface of the 0.3 pctCu-added TRIP steel during IA. The surface oxide had a discrete island morphology. Approximately 5-nm-thick oxide layer was present between the oxide islands. Si-rich xMnO·SiO$_2$ (x = 0.30) and Mn-rich xMnO·SiO$_2$ (x = 1.88) oxides were formed separately. The Si-rich oxide islands were generally thinner than the Mn-rich oxide layers. The Si-rich and Mn-rich oxides correspond to the elongated oxide island and the granular oxide layer observed in SEM (Figure 6(d)). In the cross-sectional view of the TEM sample, some part of the oxide layer appeared to be lens-shaped, as shown schematically in Figure 7(b).

Figure 11 shows cross-sectional TEM micrographs of the oxides formed the surface of the 0.05 pctSn-added TRIP steel during IA. Although the addition of Sn was very low, it resulted in a very distinct change to the morphology and the chemical composition of the oxides. As for the other TRIP steels, both Si-rich and Mn-rich xMnO·SiO$_2$ oxides were formed separately. The Si-rich oxides, however, formed lens-shaped islands

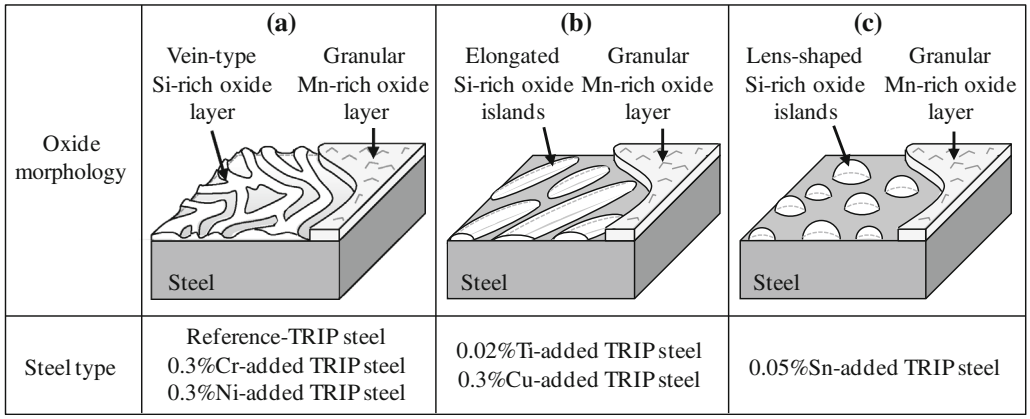

Fig. 7—Schematic drawing of the three morphologies of the oxides formed on the six TRIP steels during intercritical annealing at 1093 K (820 °C) in a N_2 + 5 pct H_2 gas atmosphere with a DP of 213 K (−60 °C). (*a*) Vein-type Si-rich xMnO·SiO$_2$ (x < 1) oxide layer and granular Mn-rich xMnO·SiO2 (x > 1) oxide layer. (*b*) Elongated Si-rich xMnO·SiO2 (x < 1) oxide islands and granular Mn-rich xMnO·SiO$_2$ (x > 1) oxide layer. (*c*) Lens-shaped Si-rich xMnO·SiO$_2$ (x < 1) oxide islands and granular Mn-rich$x$MnO·SiO$_2$ (x > 1) oxide layer.

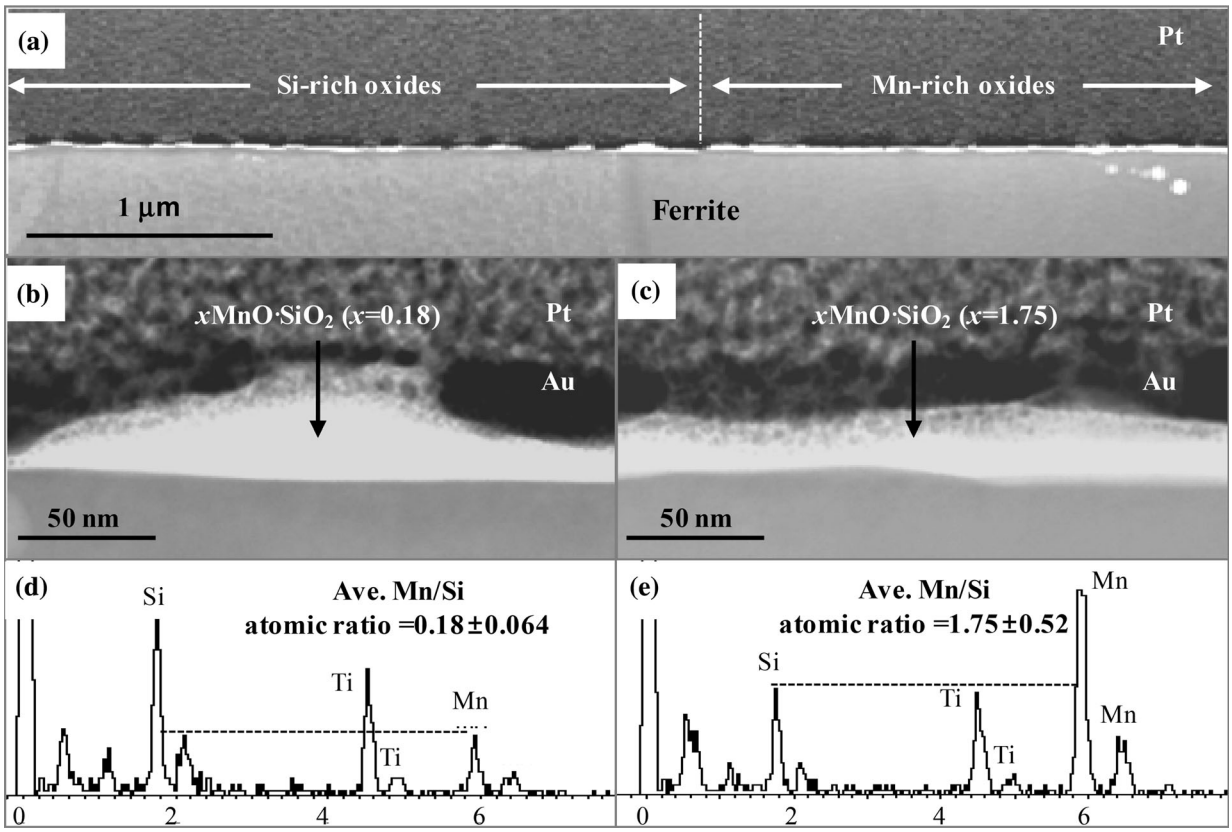

Fig. 8—TEM micrographs of the xMnO·SiO$_2$ oxides formed at the steel surface during intercritical annealing of the reference-TRIP steel at 1093 K (820 °C) in a N_2 + 5 pctH_2 gas atmosphere with a DP of 213 K (−60 °C). (*a*) Cross-sectional TEM image showing an overview of the surface. (*b*) Enlarged image of the Si-rich xMnO·SiO$_2$ (x = 0.18) oxide in (a). (*c*) Enlarged image of the Mn-rich xMnO·SiO$_2$ (x = 1.75) oxide in (a). (*d*) EDS spectrum of the Si-rich xMnO·SiO$_2$ (x = 0.18) oxide in (b). (*e*) EDS spectrum of the Mn-rich xMnO·SiO$_2$ (x = 1.75) oxide in (c).

whereas the Mn-rich oxide layers formed a continuous layer. Approximately 3-nm-thick oxide layers were present between the oxide islands. The lens shape was more pronounced than the case of the 0.3 pctCu-added TRIP steel. The average Mn/Si atomic ratio of both types of oxides was higher than for the other steels. The Mn/Si atomic ratio of the Si-rich oxides was 0.58 (Figure 11(d)), whereas those for the other TRIP steels were in the range of 0.20 to 0.30 (Figures 8 through 10). The Mn/Si atomic ratio of the Mn-rich oxides was 2.48 (Figure 11(e)), whereas it was in the range of 1.55 to 1.88 for the other steels (Figures 8 through 10). Lattice image of the Si-rich oxides indicates that they were amorphous ***a***-xMnO·SiO$_2$(x = 0.58) (Figure 11(d)). The lattice image of the Mn-rich oxides showed a clear lattice periodicity indicating that the oxides were crystalline ***c***-xMnO·SiO$_2$(x = 2.48) (Figure 11(e)). The lens-shaped morphology is believed to result in a good reactive wetting during the hot dipping of the intercritically annealed strip. This morphology provides a larger fraction of thin oxide area where Fe and the solute Al in the liquid Zn can easily react to form an inhibition layer during the hot dipping.

Figure 12 shows SIMS depth profiles for Mn and Si on the surface of the six TRIP steels. Because the area of SIMS analysis, approximately 60 μm in diameter, was much larger than nano-sized oxide particles, the results reflect the averaged contents of Mn and Si in the oxides. SIMS analysis did not show a significant difference in the oxide composition of the steels, except for 0.05 pctSn-added TRIP steel. In this case, the Si content was lower at the surface. The count level of Mn was also measured to be the highest at the surface of the 0.05 pctSn-added TRIP steel. This observation is in agreement with the TEM results which showed that the Mn content of both Si-rich and Mn-rich xMnO·SiO$_2$ oxides formed on the surface of the 0.05 pctSn-added TRIP steel was two times larger than for the oxides of the other five TRIP steels.

B. *Reactive Wetting of the Intercritically Annealed Strip*

The reactive wetting behavior was investigated by microstructural observation of the galvanized panels and by measuring the wetting force during the hot dipping. Figure 13 shows photographs of the galvanized panels intercritically annealed at 1093 K (820 °C) in a N_2 + 5 pct H_2 gas atmosphere with a DP of 213 K (−60 °C). The coating quality of the galvanized panels was significantly influenced by the addition of the minor alloying elements. Bare spots were observed on the entire surface of the galvanized panel of the reference-TRIP steel (Figure 13(a)). Many bare spots were also observed at the surface of the galvanized panel of

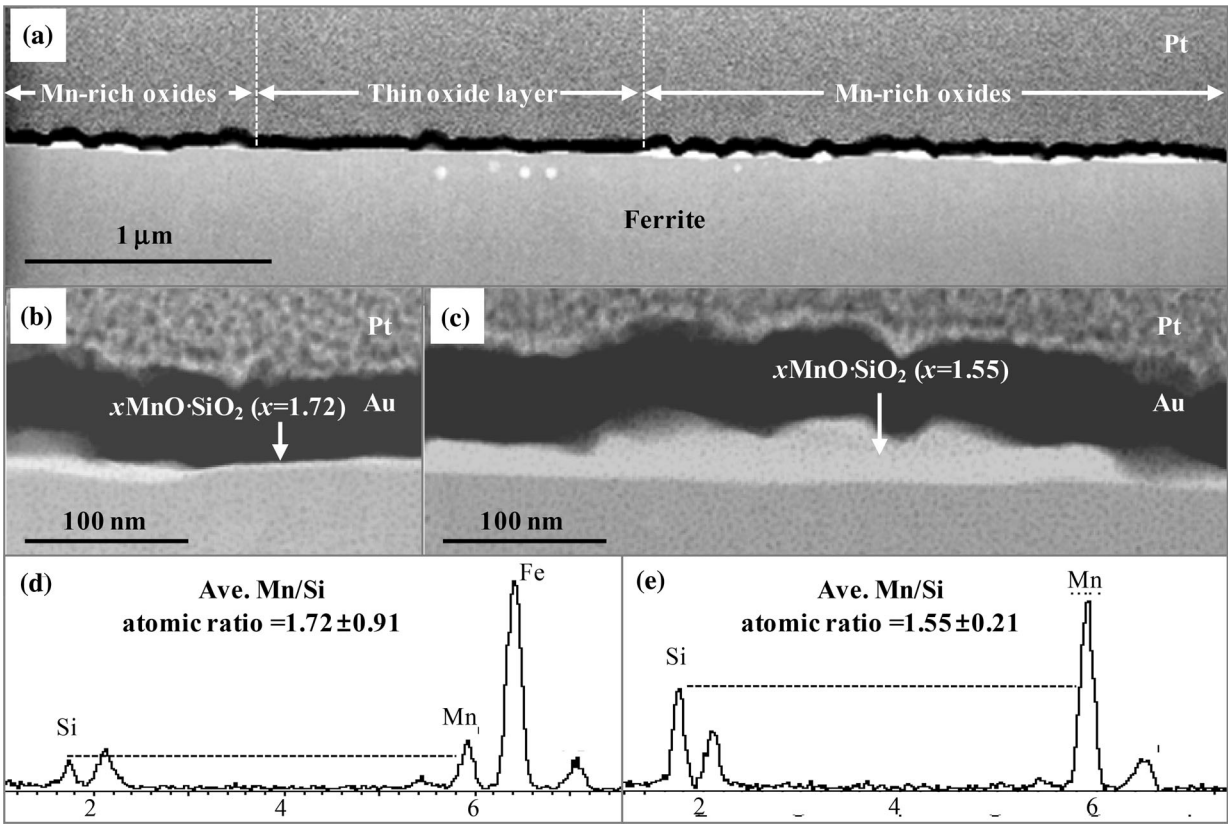

Fig. 9—TEM micrographs of the xMnO·SiO$_2$ oxides formed at the steel surface during intercritical annealing of the 0.3 pctNi-added TRIP steel at 1093 K (820 °C) in a N_2 + 5 pctH_2 gas atmosphere with a DP of 213 K (−60 °C). (*a*) Cross-sectional TEM image showing an overview of the surface. (*b*) Enlarged image of the thin oxide layer in (a). (*c*) Enlarged image of the Mn-rich xMnO·SiO$_2$ (x = 1.55) oxides in (a). (*d*) EDS spectrum of the thin oxide layer in (b). (*e*) EDS spectrum of the Mn-rich xMnO·SiO$_2$ (x = 1.55) oxide in (c).

0.3 pctCr-added TRIP steel (Figure 13(b)). The coating quality of the galvanized panels of the other steels was improved. Bare spots were observed only at the edge of the galvanized panels of the 0.02 pctTi-added TRIP steel and the 0.3 pctCu-added TRIP steel (Figures 13(d) and (e)). The quality of the entire coating surface of the galvanized panels of the 0.3 pctNi-added TRIP steel and the 0.05 pctSn-added TRIP steel was excellent.

Figure 14 shows results of wetting force measured during the hot dipping of intercritically annealed steels. Prior to the continuous annealing simulation, both sides of the samples were mirror-polished. It is interesting to note that only the surface of the 0.05 pctSn-added TRIP steel had significantly reacted with the molten Zn (Figure 14(a)). In contrast, the surface of the hot dipped samples of the other steels was clean and only a small fraction of the surface area showed traces of a reaction. The time-dependence of the normalized wetting force, $\gamma_{LV}\cos\theta$, is shown in Figure 14(b). In all cases, the wetting force had a negative value, indicating that the contact angle θ was larger than 90 deg. However, the contact angle θ for the 0.05 pctSn-added TRIP steel decreased significantly with time. This decrease of the contact angle θ implies that the steel surface was reacting with the molten Zn, resulting in an upward moving solid–liquid–vapor triple point on the sample surface during the hot dipping. The $\gamma_{LV}\cos\theta$ value did not change much during the dipping in the case of the other TRIP steels. The difference between the curves for these steels was negligible and mainly due to difference in sample edge conditions.

V. DISCUSSION

A. *Morphology and Chemical Composition of the Surface Oxide*

The suppression of carburization and decarburization reactions in steels by addition of minor alloying elements has been studied previously. S, Sb, and Sn have been reported to have the pronounced retardation effect.[19,30,31] The effect has been related to their strong tendency to segregate to the surface. This tendency is due to their large atomic size compared to Fe, which causes a strain field around the solute in the Fe lattice.[20,31] In order to release elastic energy, they diffuse from the bulk solid solution to grain boundary sites or surface sites. These elements have also been reported to effectively suppress oxidation in steels.[17,18,32] More recently, Zhang *et al.*[16,33] studied the effect of Sb addition on the oxidation behavior during recrystallization annealing of IF and TRIP steel in a N_2 + H_2 gas atmosphere containing H_2O vapor. They showed that the depth of internal oxidation decreased in Sb-alloyed steel. In these literature reports,

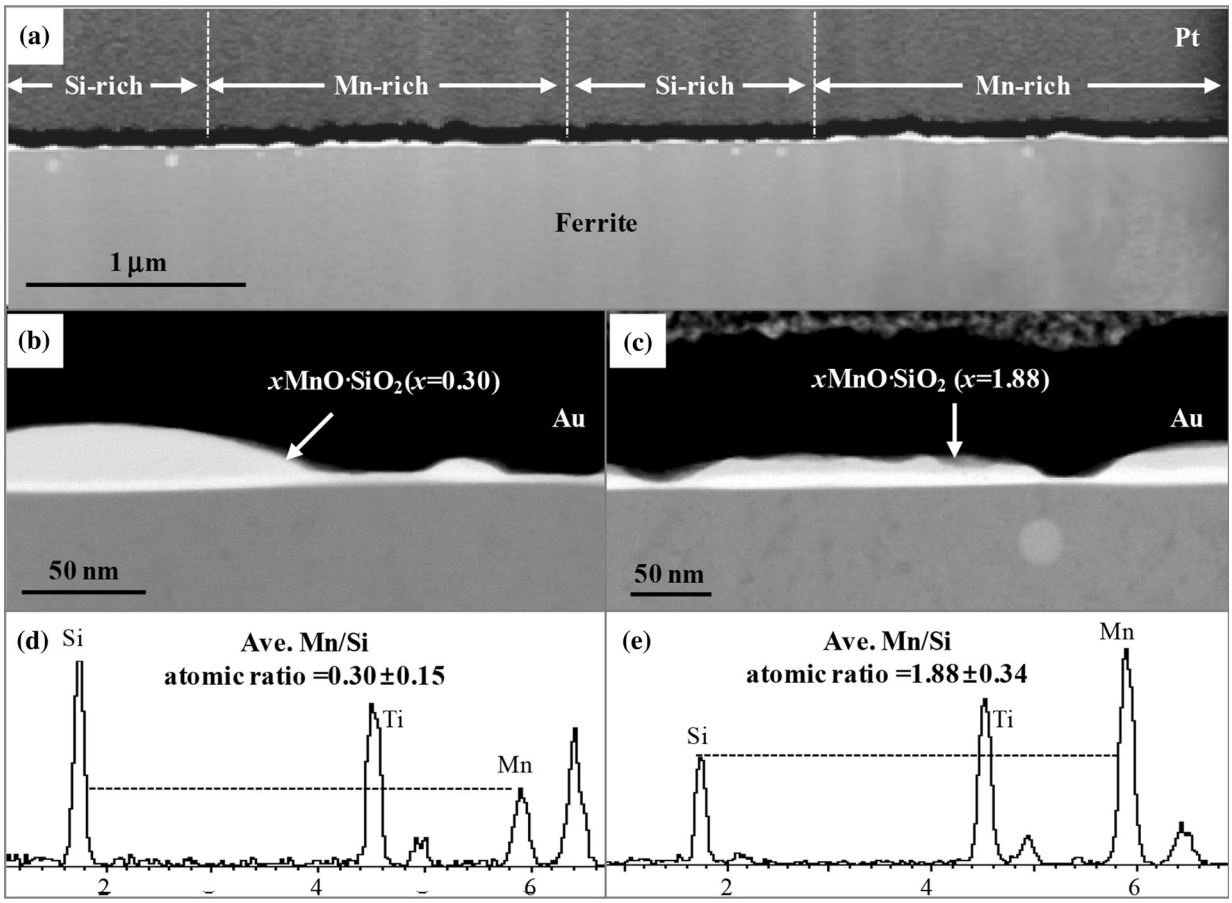

Fig. 10—TEM micrographs of the xMnO·SiO$_2$ oxides formed at the steel surface during intercritical annealing of the 0.3 pctCu-added TRIP steel at 1093 K (820 °C) in a N_2 + 5 pctH_2 gas atmosphere with a DP of 213 K (−60 °C). (*a*) Cross-sectional TEM image showing an overview of the surface. (*b*) Enlarged image of the Si-rich xMnO·SiO$_2$ (x = 0.30) oxide in (a). (*c*) Enlarged image of the Mn-rich xMnO·SiO$_2$ (x = 1.88) oxide in (a). (*d*) EDS spectrum of the Si-rich xMnO·SiO$_2$ (x = 0.30) oxide in (b). (*e*) EDS spectrum of the Mn-rich xMnO·SiO$_2$ (x = 1.88) oxide in (c).

the annealing was carried out in high temperature conditions or long annealing times, compared to the temperature and the annealing times used in industrial continuous annealing conditions.

In the present work, the effect of the surface active elements on the selective oxidation was investigated in conditions closely matching those used in industrial annealing furnaces. Although the evidence for the retardation of oxidation such as decrease in the oxide thickness was not confirmed quantitatively, it was found that a small addition of minor alloying elements effectively changed the morphology of the oxides. Continuous layer of the xMnO·SiO$_2$ oxides was formed on the surface of a reference-CMnSi TRIP steel. The layers of Mn-rich and Si-rich oxides formed separately. The continuous film morphology of the Si-rich oxides layer was changed to a discrete island morphology due to the addition of minor alloying elements. The change of the oxide morphology was associated with the degree of surface enrichment. The GDOES results were in good agreement with the degree of the surface segregation predicted by Eq. [2] (Figure 2). The degree of the surface segregation was highest for Sn (Figure 5). A considerable amount of Cu and Ti also segregated on the surface. Cr and Ni were slightly enriched at the surface. The most significant change in the morphology of the surface oxides was found for the 0.05 pctSn-added TRIP steel. The surface oxides formed on the 0.05 pctSn-added TRIP steel were lens-shaped.

This lens morphology is believed to provide a large fraction of the thin oxide area. The thin oxides are expected to be easily removed during the hot dipping. The mechanisms for the removal of the thin oxide layer during the hot dipping have already been discussed.[3,7,34,35] One mechanism is alumino-thermic reaction which is a process involving the reduction of the surface oxides by the solute Al in the Zn bath.[7,35] The other is the oxide-lift off mechanism which is a process whereby the oxides are removed from the surface into the melt by the rapid dissolution of the substrate through holes or other defects of the surface oxide.[34] Both mechanisms may contribute to the removal of the thin oxide film. In the area where oxides are removed, Fe and the solute Al in the Zn can directly react to from the $Fe_2Al_{5-x}Zn_x$ inhibition layer. The Cu and Ti additions also resulted in a change of the oxide morphology from a continuous layer to discrete islands. The Cr addition did not change the oxide morphology

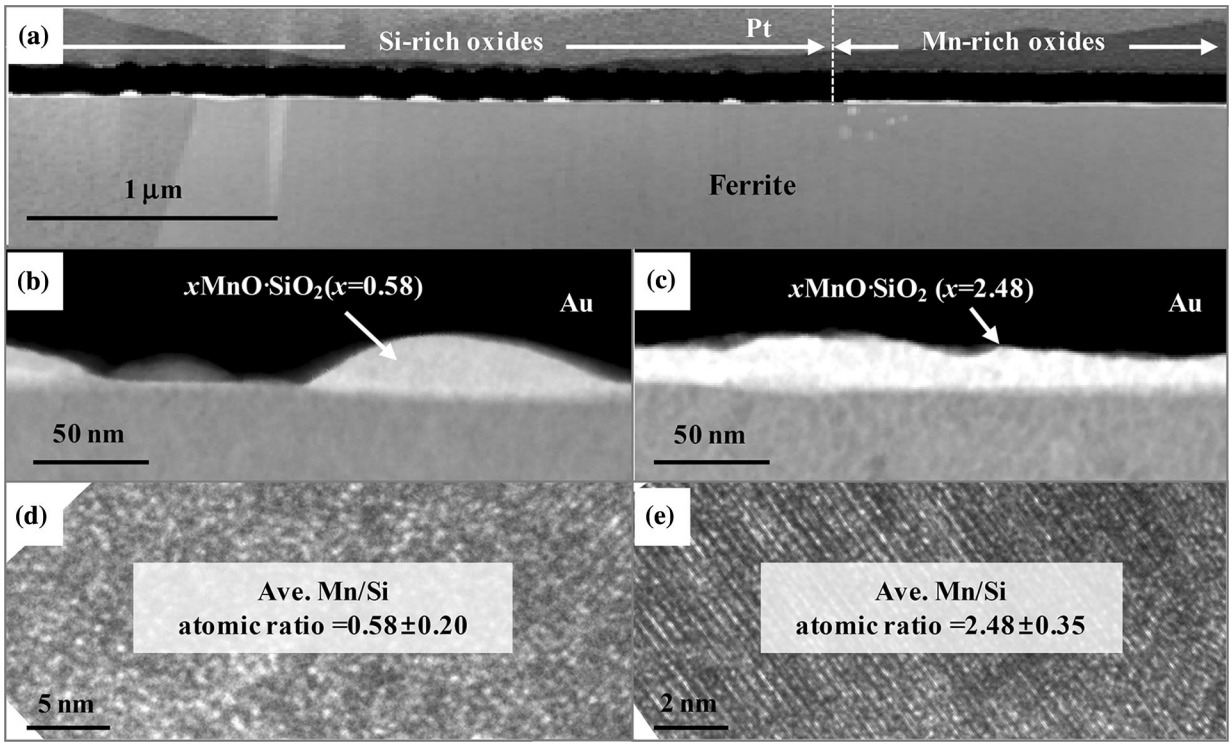

Fig. 11—TEM micrographs of the xMnO·SiO$_2$ oxides formed at the steel surface during intercritical annealing of the 0.05 pctSn-added TRIP steel at 1093 K (820 °C) in a N_2 + 5 pctH_2 gas atmosphere with a DP of 213 K (−60 °C). (*a*) Cross-sectional TEM image showing an overview of the surface. (*b*) Enlarged image of the Si-rich ***a***-xMnO·SiO$_2$ (x = 0.58) oxide in (a). (*c*) Enlarged image of the Mn-rich ***c***-xMnO·SiO$_2$ (x = 2.58) oxide in (a). (*d*) High resolution TEM image of the Si-rich ***a***-xMnO·SiO$_2$ (x = 0.58) oxide in (b). (*e*) High resolution TEM image of the Mn-rich ***c***-xMnO·SiO$_2$ (x = 2.58) oxide in (c).

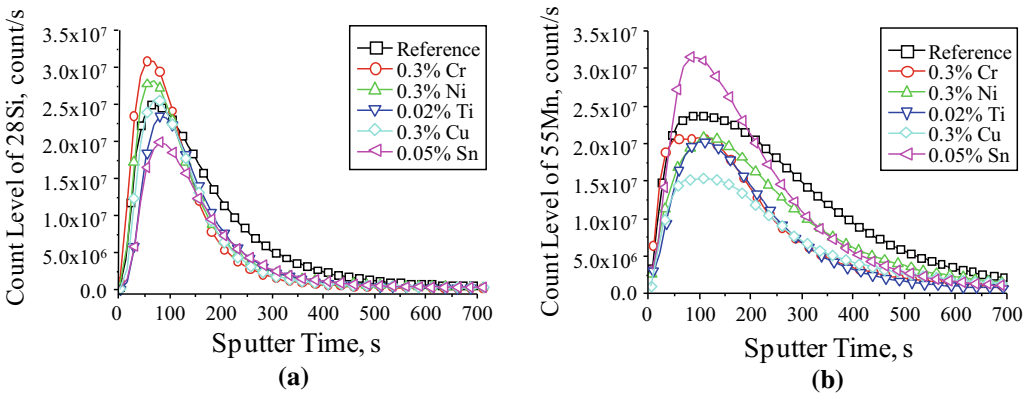

Fig. 12—SIMS depth profiles for (*a*) Si and (*b*) Mn distribution from the surface to the subsurface region of the TRIP steels.

much. Ni was an exception in terms of the relation between the degree of surface segregation and the change in the oxide morphology. Ni was found to remain in solid solution rather than segregate to the surface after annealing. It did, however, substantially alter the oxide morphology. When Ni was added, the oxide thickness was decreased, indicating that there was less oxide formation.

The mechanism for the change from a layer growth to a discrete oxide morphology when certain alloying elements were added is not clear. But, it is very likely related to the change of the oxide/steel interfacial energy. Layer-type growth is known to occur when the interaction between the atoms in the substrate and the film is larger than between adjacent atoms in the film.[36] Island-type growth occurs when interaction between atoms in the film is larger than between adjacent atoms in the film and in the substrate.[36]

In the present case, there are two main factors which can result in a change of the interface energy. One is the surface enrichment of the minor alloying elements. It is important to note that the most of minor alloying elements segregated beneath the oxide layer, *i.e.*, under the oxide/steel interface (Figure 5). There is a possibility

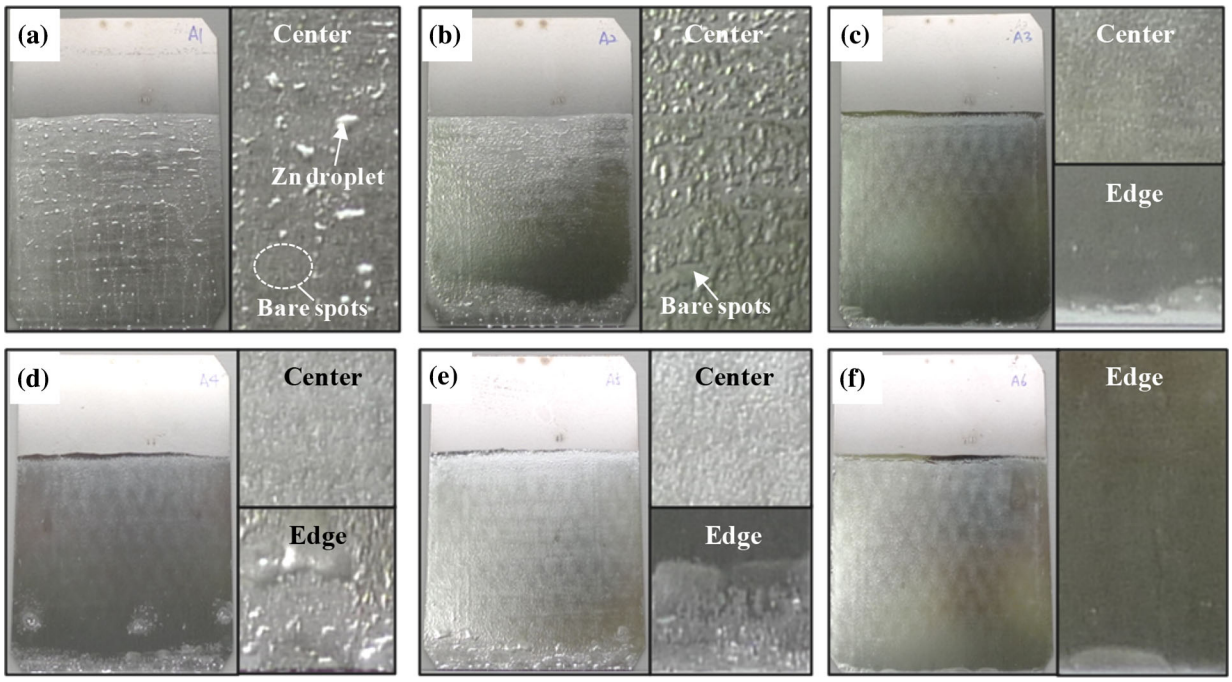

Fig. 13—Galvanized panels of (*a*) the reference-TRIP steel, (*b*) 0.3 pctCr-added TRIP steel, (*c*) 0.3 pctNi-added TRIP steel, (*d*) 0.02 pctTi-added TRIP steel, (*e*) 0.3 pctCu-added TRIP steel, and (*f*) 0.05 pctSn-added TRIP steel. The steels were intercritically annealed at 1093 K (820 °C) in a N_2 + 5 pct H_2 gas atmosphere with a DP of 213 K (−60 °C) prior to hot dipping.

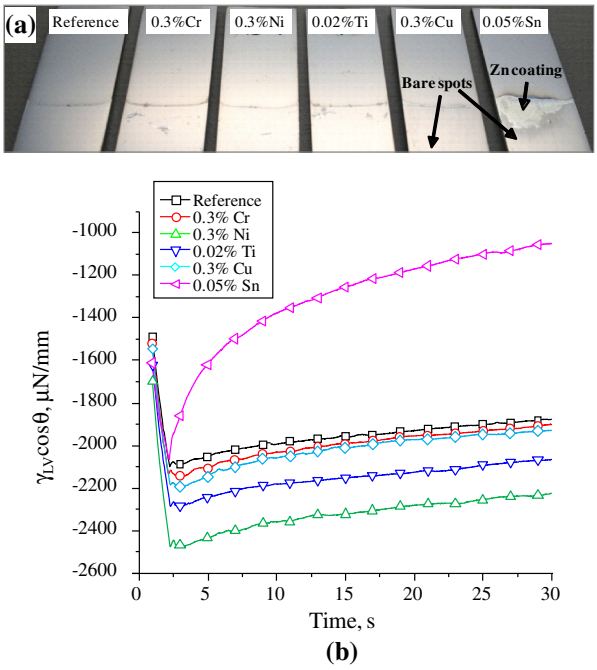

Fig. 14—(*a*) Photographs of the steel samples after reactive wetting experiments using a RHESCA force balance simulator. (*b*) Curve of the wetting force as a function of time for the six TRIP steels. The steels were intercritically annealed at 1093 K (820 °C) in a N_2 + 5 pct H_2 gas atmosphere with a DP of 213 K (−60 °C) prior to hot dipping.

that their presence changed the interfacial energy. The other possible explanation is a change in oxide chemistry. The present work showed that the addition of minor alloying elements influenced the oxide chemistry. For instance, the Mn/Si atomic ratio of the xMnO·SiO$_2$ oxides was higher at the surface of the intercritically annealed 0.05 pctSn-added TRIP steel than at the surface of the reference-TRIP steel (Figures 11 and 12). The reason for this phenomena may be explained by a mechanism which has been suggested by Zhang *et al.*[16] They reported that the depth of internal oxidation of Si during IA of TRIP steel decreased when Sb was added. Sb is a surface active element which occupies the surface adsorption sites. This results in a decrease of the oxygen permeability. To test if the same mechanism can be applied to the present case, the following experiment was carried out. Figure 15 shows SEM micrographs of the surface and the cross-sectional regions of the reference-TRIP steel and the 0.05 pctSn-added TRIP steel annealed in high gas atmosphere DP [213 K (+5 °C)] conditions. The addition of Sn affected both the external and internal oxidation. The oxide particles formed on the surface of the 0.05 pctSn-added TRIP steel were smaller than those formed on the reference-TRIP steel. The depth of internal oxidation also decreased in the Sn-added TRIP steel. The average depth of internal oxidation for the reference-TRIP steel and the 0.05 pctSn-added TRIP steel was 1.36 and 0.97 μm, respectively. These observations support the view of Zhang *et al.*,[16] that the addition of the surface active element decreases the oxygen permeability of the surface. It is well known from the work of Suzuki *et al.*[24] that the oxide chemistry is influenced by the oxidation potential. A decrease of the oxidation potential resulting from the addition of Sn may therefore have resulted in a change of the oxide/steel interfacial energy.

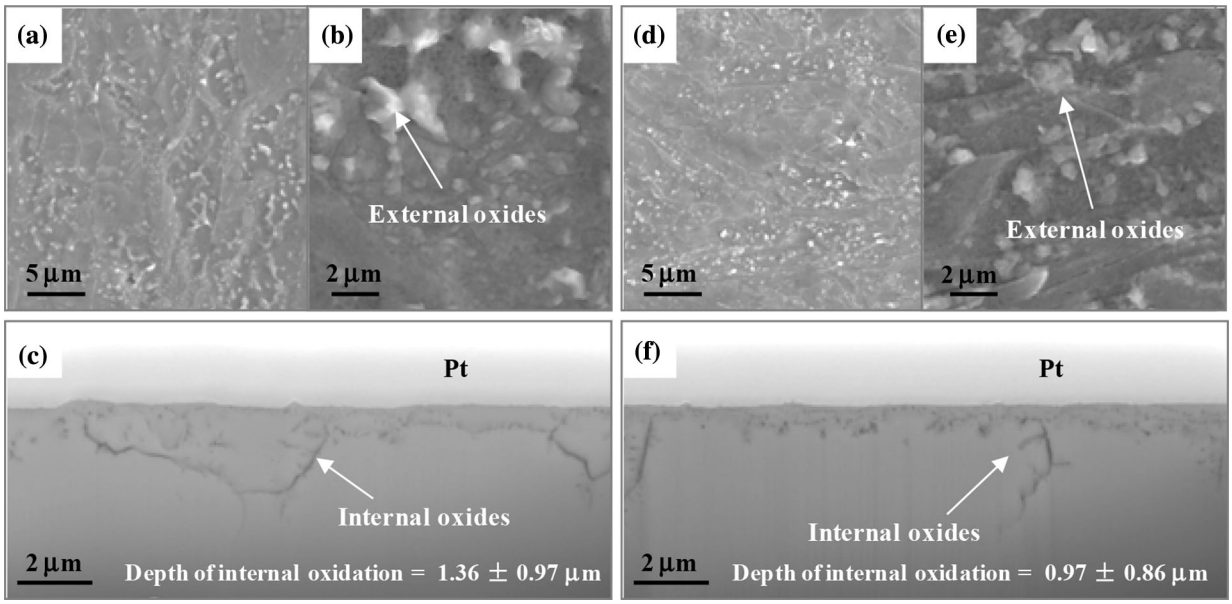

Fig. 15—SEM micrographs of the surface and subsurface of the reference-TRP steel and the 0.05 pctSn-added TRIP steel intercritically annealed at 1093 K (820 °C) in a N_2 + 10 pct H_2 gas atmosphere with a DP of 278 K (+5 °C). (*a*) SEM image of external oxides formed at the surface of the reference-TRIP steel. (*b*) Enlargement of the external oxides in Fig. 14(a). (*c*) Cross-sectional SEM image of internal oxides formed in the subsurface of the reference-TRIP steel. (*d*) SEM image of external oxides formed on the surface of the 0.05 pctSn-added TRIP steel. (*e*) Enlargement of the external oxides in Fig. 14(d). (*f*) Cross-sectional SEM image of internal oxides formed in the subsurface of the 0.05 pctSn-added TRIP steel.

The morphology of the oxides formed on the 0.3 pctNi-added TRIP steel was also significantly different from their morphology in the reference-TRIP steel, although the enrichment of Ni on the surface was found to be lowest of the alloying elements studied in this work. The oxide layers were very thin in some areas (Figure 9). The effect of Ni on the high temperature oxidation of steels containing Mn and Si was studied by Matsuno and Nishikida,[37] who found that, in the regions enriched in Ni, the oxygen solubility increased and the oxygen diffusivity decreased. Their result suggests that, in the present study, a slight enrichment of Ni on the surface may also have resulted in a decrease of the oxygen permeability at the surface which resulted in the retardation of the surface oxide formation. However, because its enrichment was very low in the present study, further work will be needed to confirm this.

B. *Reactive Wetting After Intercritically Annealing*

The galvanizability of the different TRIP steels tested in the present work was clearly related to the oxide morphology observed in SEM and TEM. Continuous oxide layers formed on the surface of the reference-TRIP steel and the 0.3 pctCr-added TRIP steel resulted in poor wetting performance, whereas discrete oxide islands formed on the surface of the 0.02 pctTi-added TRIP steel and the 0.3 pctCu-added TRIP steel resulted in improved wetting. The presence of lens-shaped oxide islands on the surface of the 0.05 pctSn-added TRIP steel resulted in the best wettability. Although the oxide layer formed on the surface of the 0.3 pctNi-added TRIP steel was continuous, *i.e.*, similar to the case of the reference-TRIP steel, it was very thin. The reduced oxide film thickness also resulted in an improved wetting.

Both the galvanizing simulations and the wetting force measurements confirmed that Sn additions improved the wettability of the intercritically annealed steels. There were, however, essential differences between the two experimental results. The results for the galvanizing simulation showed that addition of small amounts of Ni, Ti, Cu, and Sn improved the galvanizability whereas the results for wetting force measurement indicated that the reactive wetting occurred only for the 0.05 pctSn-added TRIP steel. An additional difference was that the reaction between the steel surface and the molten Zn was slower during the wetting force measurement than during the galvanizing simulation, although the reaction times for the wetting experiments were much longer. This may be due to the different experimental conditions as the samples used for the wetting experiments were polished prior to the simulation. In addition, different equipment was used for the galvanizing simulations and the wetting experiments and the annealing conditions were also slightly different.

The formation of lens-shaped oxides on the surface of the 0.05 pctSn-added TRIP steel improved wetting of the intercritically annealed steel by the molten Zn (Figures 13 and 14). The advantage of this oxide morphology with respect to wettability is that it provides a large area between the oxide particles, where the $Fe_2Al_{5-x}Zn_x$ inhibition layer can be formed. Bellhouse and McDermid[7] also stressed the importance of the influence of the morphology of the surface oxides on the wettability. They showed that when closely spaced

nodules of surface oxides were formed during IA of a TRIP steel, the number of bare spot defects increased.

The galvanizability and the wettability of 0.3 pctCr-added TRIP steel by molten Zn were not improved. The enrichment of Cr near the surface was detected by GDOES. As Cris itself subject to selective oxidation and forms Cr_2O_3 oxide during annealing, it will accelerate external oxidation. The effect of Cr is comparable to the effect of B, which has a high surface segregation tendency, but accelerates the surface oxidation.[33]

VI. CONCLUSIONS

The influence of minor additions of Cr, Ni, Ti, Cu, and Sn on the selective oxidation and the reactive wetting of CMnSi TRIP steels was studied using laboratory galvanizing simulations. Five TRIP steels containing Cr, Ni, Ti, Cu, and Sn were investigated. After annealing at 1093 K (820 °C) in a N_2 + 5 pctH_2 gas atmosphere with a DP of 213 K (−60 °C), two types of the surface oxides were formed separately: Mn-rich xMnO·SiO_2 ($x > 1.5$) and Si-rich xMnO·SiO_2 ($x < 0.3$) oxides. The small alloying additions changed the morphology of the Si-rich xMnO·SiO_2 ($x < 0.3$) oxides layers from continuous films to discrete islands. It is proposed that the alloying elements segregated to the surface during annealing and thereby reduced the oxygen permeability of the surface. This led to a change of the composition of the xMnO·SiO_2 oxides and the oxide/matrix interfacial energy.

The formation of a continuous oxide layer on the surface of the reference-TRIP steel and the 0.3 pctCr-added TRIP steel resulted in a poor wetting by the liquid Zn. The formation of elongated oxide islands on the surface of the 0.02 pctTi-added TRIP steel and the 0.3 pctCu-added TRIP steel resulted in an improved wetting. The formation of characteristic lens-shaped oxide islands on the surface of the 0.05 pctSn-added TRIP steel resulted in excellent wetting properties of the panels and a defect-free Zn coating after solidification. The oxide layer formed on the surface of the 0.3 pctNi-added TRIP steel was continuous and very thin. This also resulted in a good wettability. The improved Zn wetting of the TRIP steels with small alloying additions of Cu, Ti, Ni, and Sn was attributed to an increased surface area fraction where the oxides are thinner, so that Fe and the Al can easily react to form the $Fe_2Al_{5-x}Zn_x$ inhibition layer during the galvanizing. Addition of minor alloying elements can therefore significantly contribute to the decrease of Zn-coating defects on CMnSi TRIP steels processed in HDG lines.

The following characteristics are necessary conditions for a surface reactive element to suppress selective oxidation and improve the galvanizability of TRIP steel:

1. The element should have strong tendency to segregate to the surface. Alloying elements with larger atomic size compared to Fe have a positive effect on galvanizability.
2. The element should not be selectively oxidized in the annealing atmosphere.
3. The element should also be present as a solute and not form precipitates.

On the basis of these criteria, elements such as S, As, Sb, and Bi are potentially as effective as Sn to improve the galvanizability of Si-containing TRIP steel.

ACKNOWLEDGMENTS

The authors gratefully acknowledge the support of POSCO. The suggestions of Dr. Kwang Soo Shin of RIST (Pohang, Korea) on the interpretation of the results reported in the manuscript are highly appreciated.

REFERENCES

1. Y.F. Gong, H.S. Kim, and B.C. De Cooman: *ISIJ Int*., 2008, vol. 48, pp. 1745–51.
2. Y.F. Gong, H.S. Kim, and B.C. De Cooman: *ISIJ Int*., 2009, vol. 49, pp. 557–63.
3. L. Cho, S. Lee, M. Kim, Y. Kim, and B.C. De Cooman: *Metall. Mater. Trans. A*, 2013, vol. 44A, pp. 362–71.
4. K.K. Wang, C.W. Hsu, L. Chang, D. Gan, and K.C. Yang: *Appl. Surf. Sci*., 2013, vol. 285, pp. 458–68.
5. I. Cvijović, I. Parezanović, and M. Spiegel: *Corros. Sci*., 2006, vol. 48, pp. 980–93.
6. H. Liu, F. Li, W. Shi, S. Swaminathan, Y. He, M. Rohwerder, and L. Li: *Surf. Coat. Technol*., 2012, vol. 206, pp. 3428–36.
7. E.M. Bellhouse and J.R. McDermid: *Metall. Mater. Trans. A*, 2010, vol. 41A, pp. 1539–53.
8. L. Cho, M.S. Kim, Y.H. Kim, S.J. Lee, B.C. De Cooman: *Proceedings of the 8th International Conference on Zinc and Zinc Alloy Coated Steel Sheet (GALVATECH 2011)*, Genova, Italy, 2011, Associazione Italiana di Metallurgia, pp. 145–52.
9. R. Nakanishi, H. Irie, M. Nakamura, K. Okamoto, and M. Shimizu: European Patent, EP 1829 983 (A1), 2007.
10. L. Bordignon, X.V. Eynde, and R. Franssen: *Rev. Métall*., 2004, vol. 101, pp. 559–68.
11. M. Blumenau, M. Norden, F. Friedel, and K. Peters: *Surf. Coat. Technol*., 2011, vol. 206, pp. 559–67.
12. Y.F. Gong and B.C. De Cooman: *ISIJ Int*., 2011, vol. 51, pp. 630–37.
13. Y.I. Choi, W.J. Beom, C.J. Park, D. Paik, and M.H. Hong: *Metall. Mater. Trans. A*, 2010, vol. 41A, pp. 3379–85.
14. R. Sanguanmoo, E. Nisaratanaporn, and Y. Boonyongmaneerat: *Corros. Sci*., 2011, vol. 53, pp. 122–26.
15. T. Matsumoto: *CAMP-ISIJ*, 1991, vol. 4, p. 1632.
16. Z.T. Zhang, I.R. Sohn, F.S. Pettit, G.H. Meier, and S. Sridhar: *Metall. Mater. Trans. B*, 2009, vol. 40B, pp. 567–84.
17. E. Clauberg, C. Uebing, and H. Grabke: *Appl. Surf. Sci*., 1999, vol. 143, pp. 206–214.
18. G. Lyudkovsky: United States Patent, No. 4,421,574, 1983.
19. A. Ruck, D. Monceau, and H.J. Grabke: *Steel Res*., 1996, vol. 67, pp. 240–46.
20. M. Seah: *Acta Metall*., 1980, vol. 28, pp. 955–62.
21. N. Tsai, G. Pound, and F.F. Abraham: *J. Catal*., 1977, vol. 50, pp. 200–202.
22. D.R. Lide: *CRC Handbook of Chemistry and Physics*, 86th ed., CRC Press, Boca Raton, 2005.
23. H.G. Lee: *Chemical Thermodynamics for Metals and Materials*, Imperial College Press, London, 1999.
24. Y. Suzuki, T. Yamashita, Y. Sugimoto, S. Fujita, and S. Yamaguchi: *ISIJ Int*., 2009, vol. 49, pp. 564–73.
25. T. Iung, O. Faral, M. Faral, M. Babbit, and C. Issartel: United States Patent 6328826 B1, 2001.
26. K. Takashima, Y. Toji, and K. Hasegawa: United States Patent 20130340898 A1, 2013.

27. D. Melford: *Philos. Trans. R. Soc. Lond. A*, 1980, vol. 295, pp. 89–103.
28. D. Huin, P. Flauder, and J.B. Leblond: *Oxid. Met.*, 2005, vol. 64, pp. 131–67.
29. S. Alibeigi, R. Kavitha, R.J. Meguerian, and J.R. McDermid: *Acta Mater.*, 2011, vol. 59, pp. 3537–49.
30. D. Sain and G. Belton: *Metall. Trans. B*, 1978, vol. 9B, pp. 403–407.
31. H.J. Grabke: *Kovine zlitine tehnologije*, 1996, vol. 30, pp. 483–95.
32. H. Grabke, R. Dennert, and B. Wagemann: *Oxid. Met.*, 1997, vol. 47, pp. 495–506.
33. Y.Y. Zhang, Y.Y. Zhang, F.H. Yang, and Z.T. Zhang: *J. Iron. Steel Res. Int.*, 2013, vol. 20, pp. 39–56.
34. N. Gao, D.Y.H. Liu, N. Tang, R.B. Park, and M.S. Kim: *Proceedings of the 8th International Conference on Zinc and Zinc Alloy Coated Steel Sheet (GALVATECH 2011)*, Genova, Italy, 2011, Associazione Italiana di Metallurgia, pp. 123–30.
35. R. Kavitha and J.R. McDermid: *Surf. Coat. Technol.*, 2012, vol. 212, pp. 152–58.
36. N. Kaiser: *Appl. Opt.*, 2002, vol. 41, pp. 3053–60.
37. F. Matsuno and S. Nishikida: *Tetsu-to-Hagane*, 1982, vol. 68, pp. 301–308.